

Spin-orbit coupling, strong correlation, and insulator-metal transitions: the $J_{\text{eff}} = \frac{3}{2}$ ferromagnetic Mott insulator $\text{Ba}_2\text{NaOsO}_6$

Shruba Gangopadhyay and Warren E. Pickett

Department of Physics, University of California, Davis CA 95616, USA

(Dated: October 14, 2014)

The double perovskite $\text{Ba}_2\text{NaOsO}_6$ (BNOO), an exotic example of a very high oxidation state (heptavalent) osmium d^1 compound and also uncommon by being a ferromagnetic Mott insulator without Jahn-Teller (JT) distortion, is modeled using the density functional theory (DFT) hybrid functional based exact exchange for correlated electrons (oeHyb) method and including spin-orbit coupling (SOC). The experimentally observed narrow gap ferromagnetic insulating ground state is obtained, with easy axis along [110] in accord with experiment, providing support that this approach provides a realistic method for studying this system. The predicted spin density for [110] spin orientation is nearly cubic (unlike for other directions), providing an explanation for the absence of JT distortion. An orbital moment of $-0.4\mu_B$ strongly compensates the $+0.5\mu_B$ spin moment on Os, leaving a strongly compensated moment more in line with experiment. Remarkably, the net moment lies primarily on the oxygen ions. An insulator-metal transition by rotating the magnetization direction with an external field under moderate pressure is predicted as one consequence of strong SOC, and metallization under moderate pressure is predicted. Comparison is made with the isostructural, isovalent insulator $\text{Ba}_2\text{LiOsO}_6$ which however orders antiferromagnetically.

PACS numbers:

I. INTRODUCTION

Over the last three decades the orbital physics of d^1 systems and its interplay with spin has focused primarily on transition metal oxides, especially $3d$ transition metals (TMs). While the magnetic d^1 configuration has been studied mostly in $3d$ systems, it can also occur in mid-to late- $5d$ TM ionic systems. For these heavy ions spin-orbit coupling (SOC) becomes a competing factor, mixing the various spin, orbital, charge, and lattice degrees of freedom. The interplay of strong electron correlation and large SOC is relatively less explored, and certainly not well understood at all, because the behavior involves so many comparable energy scales. This situation arises in a broad family of magnetic Mott insulating systems in which three-fold degenerate t_{2g} orbitals are partially filled.¹ In such systems orbital degeneracy is protected only by cubic lattice symmetry, and typically the crystal field splitting is large enough that e_g orbitals are out of the picture.

In $5d$ t_{2g} subshells where SOC remains unquenched (cubic symmetry), the six one-electron levels split into an upper $J=1/2$ doublet and a lower $J=3/2$ quartet. In this category Ir-based based magnets have been studied actively.²⁻⁶ A prominent class of such systems is the ordered double perovskites, with chemical formula $\text{A}_2\text{BB}'\text{O}_6$. We are interested in the case where B is a closed shell cation and B' is a magnetic ion; in such cases unusually high formal valence states can arise. A few examples attracting recent interest are $\text{B}'=\text{Ru}^{5+}$ and Os^{5+} in $\text{A}_2\text{NaB}'\text{O}_6$ ($\text{A}=\text{La}$ and Nd),⁷⁻⁹ Mo^{5+} in Ba_2YMoO_6 , Os^{6+} in $\text{Ba}_2\text{CaOsO}_6$,¹⁰ and heptavalent Os in Ba_2BOsO_6 ($\text{B}=\text{Li}, \text{Na}$). If we narrow our focus to d^1 B' ions only, the possibilities are practically confined to Mo^{5+} , Re^{6+} and Os^{7+} . Song *et al.* have reported a theoretical study¹¹ of KO_4 with heptavalent Os, where large SOC,

strong correlations, and structural symmetry breaking conspire to produce an unexpectedly large orbital moment in the e_g^1 shell that nominally supports no orbital moment.

The recently studied compounds^{12,13} Ba_2BOsO_6 ($\text{B}=\text{Li}, \text{Na}$) show many features to make them of current interest. Besides the double-perovskite structure, and being a rare example of a heptavalent osmium compound, $\text{Ba}_2\text{NaOsO}_6$ (BNOO) is exotic in being a *ferromagnetic Mott insulator*,^{13,14} with order appearing at $T_C = 6.8\text{K}$ with Curie-Weiss temperature $\Theta_{CW} = -10\text{K}$. Although its single t_{2g} electron orders magnetically, it shows no evidence of the anticipated orbital order that causes Jahn-Teller distortion and should destroys its cubic symmetry. The sister compound $\text{La}_2\text{NaOsO}_6$, on the other hand, with high-spin d^3 Os configuration and a nominally cubic symmetry, is observed to be highly distorted.¹⁵ This distortion is ascribed to geometrical misfit arising from incompatible ionic radii.

There is a recent example of an Os-based based $5d^4$ perovskite compound BaOsO_3 that remains cubic;¹⁶ on the other hand a related perovskite $5d^5$ NaOsO_3 does distort.¹⁷ The question of origin of the magnetic ordering in BNOO is surely a delicate one, since isostructural, isovalent, and also Mott insulating $\text{Ba}_2\text{LiOsO}_6$ (BLOO) orders *antiferromagnetically* in spite of a very similar Curie-Weiss susceptibility¹⁴ and similar volume.

Lee and Pickett demonstrated¹⁸ that, before considering magnetism and on-site interaction effects, SOC splits the t_{2g} bands into a lower $J=\frac{3}{2}$ quartet and an upper $J=\frac{1}{2}$ doublet, as expected. Since BNOO is observed to be insulating and effects of spin-orbit coupling drive the behavior, it provides the first " $J_{\text{eff}}=\frac{3}{2}$ " Mott insulator at quarter-filling, analogous to the " $J_{\text{eff}}=\frac{1}{2}$ " Mott insulators at half-filling that are being studied in $5d^5$ systems.^{5,19,20}

Including spin polarization and on-site Hubbard U

repulsion beyond the semilocal density approximation (DFT+U+SOC) with both the Wien2k and FPLO codes gave essentially full spin polarization but was not able to open a gap¹⁸ with a reasonable value of U . The complication is that the occupied orbital is a OsO_6 cluster orbital with half of the charge on Os and the other half spread over the neighboring O ions. U should be a value appropriate to this cluster orbital and should be applied to that orbital, however the codes applied U only to the Os $5d$ orbitals. Xiang and Whangbo²¹ neglected the Hund's rule J_H in the DFT+U method, and did obtain a gap. However, neglecting J_H omits both the Hund's rule exchange energy and the anisotropy (orbital dependence) of the Hubbard interaction $U_{mm'}$, whereas one of our intentions is to include all orbital dependencies to understand the anisotropy on the Os site.

In this paper we first establish how to model this system faithfully including all anisotropy, then address the interplay of SOC coupling with correlation effects and crystal field splitting. The density functional extension to include some fraction of Hartree-Fock exchange – the hybrid functional – open the gap, but only when SOC is included. The inclusion of nonlocal exchange and SOC provides an understanding of the Mott insulating ground state and a $[110]$ easy axis, both in agreement with experimental data.¹³ We conclude that BNOO provides an example of a $J_{\text{eff}} = \frac{3}{2}$, quarter-filled Mott insulator. Some comparison is made to isovalent BLOO, which had 6% smaller volume and aligns antiferromagnetically rather than ferromagnetically.

II. PREVIOUS THEORETICAL WORK

Two density functional theory based studies, mentioned briefly above, have been reported for BNOO. One was performed within a fully anisotropic implementation of the DFT+U method¹⁸ while the other was DFT+U²¹ (GGA+U), but neglecting anisotropy of the interaction. An overriding feature of this system is a strong hybridization of Os $5d$ orbitals with O $2p$ states, with the result that the “ t_{2g} ” bands have half of their density on the four neighboring oxygen ions in the plane of the orbital. In keeping with this strong hybridization, the “O $2p$ ” bands have considerable Os $5d$ charge, such that the $5d$ occupation of the nominally d^1 ion is actually 4-5 electrons, still leaving a highly charged ion but less than half of the formal $7+$ designation. Lee and Pickett reported¹⁸ that fully anisotropic DFT+U could not reproduce a Mott insulating state because U is applied on the Os ion whereas half of the occupied local orbital (cluster orbital) density lies on neighboring oxygen ions. A model treatment in which U is applied to the cluster orbital did produce the Mott insulating state.¹⁸ Whangbo's results indicate that part of the complication in this system involves the anisotropy of the repulsion within the Os ion.

The study reported by Whangbo *et. al.*²¹ addressed three spin directions ($[001]$, $[110]$, and $[111]$). Within their treatment, the $[111]$ spin direction led to the min-

imum energy, indicated a calculated band gap of 0.3 eV for $U=0.21 \text{ Ry} = 2.85 \text{ eV}$ ($J_H=0$). Using DFT+U+SOC and the same code but including anisotropy of the interaction $U_{mm'}$, we have not reproduced this gap, indicating their gap is due to the neglect of Hund's rule coupling and anisotropy of the interaction. Because of the need to include all interactions and all anisotropy, we have adopted a different approach based on the hybrid exchange-correlation functional, described in the next section. This approach seems to be more robust, allowing us to probe the interplay of SOC and strong correlation of BNOO, and also obtain results of the effect of pressure on the ground state of BNOO.

Our first challenge was to obtain a Mott insulating state in BNOO when all interactions (correlation and SOC) are accounted for. With large SOC the result depends on the assigned direction of the moment. The hybrid functional approach plus SOC leads directly to a ferromagnetic (FM) Mott insulating ground state, as observed.¹³ In our studies we observed a strong preference for FM alignment, versus the commonplace antiferromagnetic (AFM) alignment that often arises on the simple cubic lattice of perovskite oxides. $\text{Ba}_2\text{LiOsO}_6$ however orders antiferromagnetically, which for nearest neighbor antialignment exchange coupling leads to frustration of ordering. All calculations reported here for either compound are for FM orientation. We study specifically the effects of spin orientation on the electronic structure, and initiate a study of the pressure dependence of BNOO considering the zero pressure lattice constant and at 1%, 2%, and 5% reduced lattice constants.

III. COMPUTATIONAL METHODS

The present first-principles DFT-based electronic structure calculations were performed using the full-potential augmented plane wave plus local orbital method as implemented in the WIEN2k code.²² The structural parameters of BNOO with full cubic symmetry of the double perovskite structure were taken from experimental X-ray crystallographic data:¹⁴ $a=8.28 \text{ \AA}$, $x_O=0.2256$. Non-overlapping atomic sphere radii of 2.50, 2.00, 1.80, and 1.58 a.u. are used for the Ba, Na, Os, and O atoms, respectively. The Brillouin zone was sampled with a minimum of 400 k points during self-consistency, coarser meshes were sometimes found to be insufficient.

For the exchange-correlation energy functional for treating strongly correlated insulators, a variety of approaches in addition to DFT+U exist and have been tested and compared for a few selected systems.²³ As mentioned above, for technical reasons – the relevant orbital is an octahedron cluster orbital rather than the standard localized, atomic-like orbital encountered in $3d$ oxides – the LDA+U method is problematic. We have chosen to apply the onsite exact exchange for correlated electrons (EECE) functional introduced and evaluated by Novak and collaborators.²⁴, implemented similarly to common use in hybrid (mixture of Hartree-Fock and lo-

cal density exchange). This oeeHyb functional is an extension of the DFT+U method to parameter-free form: exact exchange with full anisotropy is evaluated for correlated orbitals (Os $5d$ orbitals here) without explicit reference to any (screened or unscreened) Hubbard U repulsion or Hund's exchange interaction J_H . The double counting term is evaluated directly from the density of the occupied correlated orbitals, again without any input parameters. The exact exchange is calculated within the atomic sphere in atomic-like fashion (hence "onsite"). The onsite exact exchange replaces 25% of the local density exchange.

This functional is implemented in the Wien2k code,²⁵ and we refer to it here as oeeHyb. For the semilocal exchange-correlation functional, the parametrization of Perdew, Burke, and Ernzerhof²⁶ (generalized gradient approximation) is used. SOC was included fully in core states and for valence states was included in a second-variational method using scalar relativistic wave functions,³⁰ a procedure that is non-perturbative and quite accurate for d orbitals even with large SOC.

This oeeHyb method has some kinship with hybrid exchange-correlation functionals (see Tran *et al.*²³ for a comparison of several hybrids). Hybrids replace some fraction α , typically 25%, of local density exchange with Hartree-Fock exchange, which then is approximated in various ways to reduce the expense to a reasonable level. The oeeHyb approach deals with exact exchange only for correlated orbitals, however, making it appropriate for correlated materials but it will not increase bandgaps of ionic or covalent semiconductors.

We note that as an alternative to the commonly used DFT+U approach, the more conventional hybrid exchange-correlation functional as implemented in the VASP code²⁸ has been applied to the iridate Na_2IrO_3 by Kim *et al.*²⁹ to obtain the magnetic insulating ground state.

IV. ELECTRONIC STRUCTURE AND MAGNETIC MOMENTS

A. Electronic structure: dependence on spin direction

Projected densities of states (PDOSs) are presented in Fig. 1 for BNOO at the experimental volume using oeeHyb, initially without SOC and with full cubic symmetry. The Fermi level (taken as the zero of energy) lies in a deep pseudogap, due to small band overlap. All t_{2g} orbitals participate equally at this level, evident from the observation that the PDOS is distributed almost equally over the Os t_{2g} orbitals and the $2p$ orbitals of the six neighboring O ions, a very strong hybridization effect that has been emphasized before.¹⁸

The conventional picture of a Mott insulating state in a t_{2g}^1 shell is that a single orbital, say d_{xy} , is occupied, and the crystal symmetry is broken (and must be broken in the calculation) to sustain, indeed to allow, occupation of

Method	μ_s	μ_l	μ_{tot}	Band Gap
Lattice parameter 8.28 Å				
oeeHyb	0.59	N/A	N/A	none
oeeHyb+SOC (001)	0.52	-0.41	0.11	0.02
oeeHyb +SOC (110)	0.52	-0.44	0.08	0.28
oeeHyb +SOC (111)	0.52	-0.45	0.07	0.30
Lattice parameter 8.20 Å				
oeeHyb	0.53	N/A	N/A	none
oeeHyb+SOC (001)	0.49	-0.37	0.11	none
oeeHyb +SOC (110)	0.48	-0.41	0.08	0.21
oeeHyb +SOC (111)	0.48	-0.42	0.06	0.26
lattice parameter 8.10 Å				
oeeHyb	0.51	N/A	N/A	none
oeeHyb+SOC (001)	0.48	-0.37	0.12	none
oeeHyb +SOC (110)	0.48	-0.27	0.21	0.12
oeeHyb +SOC (111)	0.48	-0.35	0.13	0.15
Lattice parameter 7.86 Å				
oeeHyb	0.48	N/A	N/A	none
oeeHyb +SOC (001)	0.46	-0.34	0.12	none
oeeHyb +SOC (110)	0.47	-0.38	0.09	none
oeeHyb +SOC (111)	0.47	-0.39	0.09	none

TABLE I: Calculated spin, orbital, and total ($\mu_{tot}=\mu_s+\mu_l$) moments of Os, and band gap of $\text{Ba}_2\text{NaOsO}_6$, for four values of lattice parameter and for the three high symmetry directions of the magnetization. Note: the total moment per f.u. will include an $\sim 0.5\mu_B$ spin moment not included within the Os sphere, thus primarily on the oxygen ions.

a single orbital. However, due to the large SOC which is expected to produce a substantial orbital moment which requires occupation of a complex (*viz.* $d_{xz} \pm id_{yz}$) orbital, we have foregone this intermediate step of obtaining orbital-ordering broken symmetry, which would typically be the final result for a $3d$ ion with negligible SOC.

Adding SOC to oeeHyb, the result mentioned above, which necessarily lowers the symmetry, leads to a SOC-driven Mott insulating state with a 0.2-0.3 eV gap, depending on the direction assumed for the magnetization. It is for this reason that we use the oeeHyb functional to model BNOO, as we have previously reported that the LDA+U approach was unable to open a gap.¹⁸ The GGA+U method is more promising, but it requires an unphysically large value of $U = 6$ eV to open a gap for [001] orientation. One can obtain a band gap along for [110] and [111] orientations in GGA+U with U values of 3.2 eV and 2.0 eV, respectively.³¹

Our calculated band gaps, provided in Table I, depend on direction of the magnetization, which experimentally can be manipulated with an applied field. It should be kept in mind that symmetry is lowered by including SOC, and the resulting symmetry depends on the direction of magnetization. For spin along [001] the band gap is lower by 70 meV than for [110] and [111].

In the d^1 Mott insulating state a single (Wannier) orbital is occupied. While SOC mixes spins, the split-

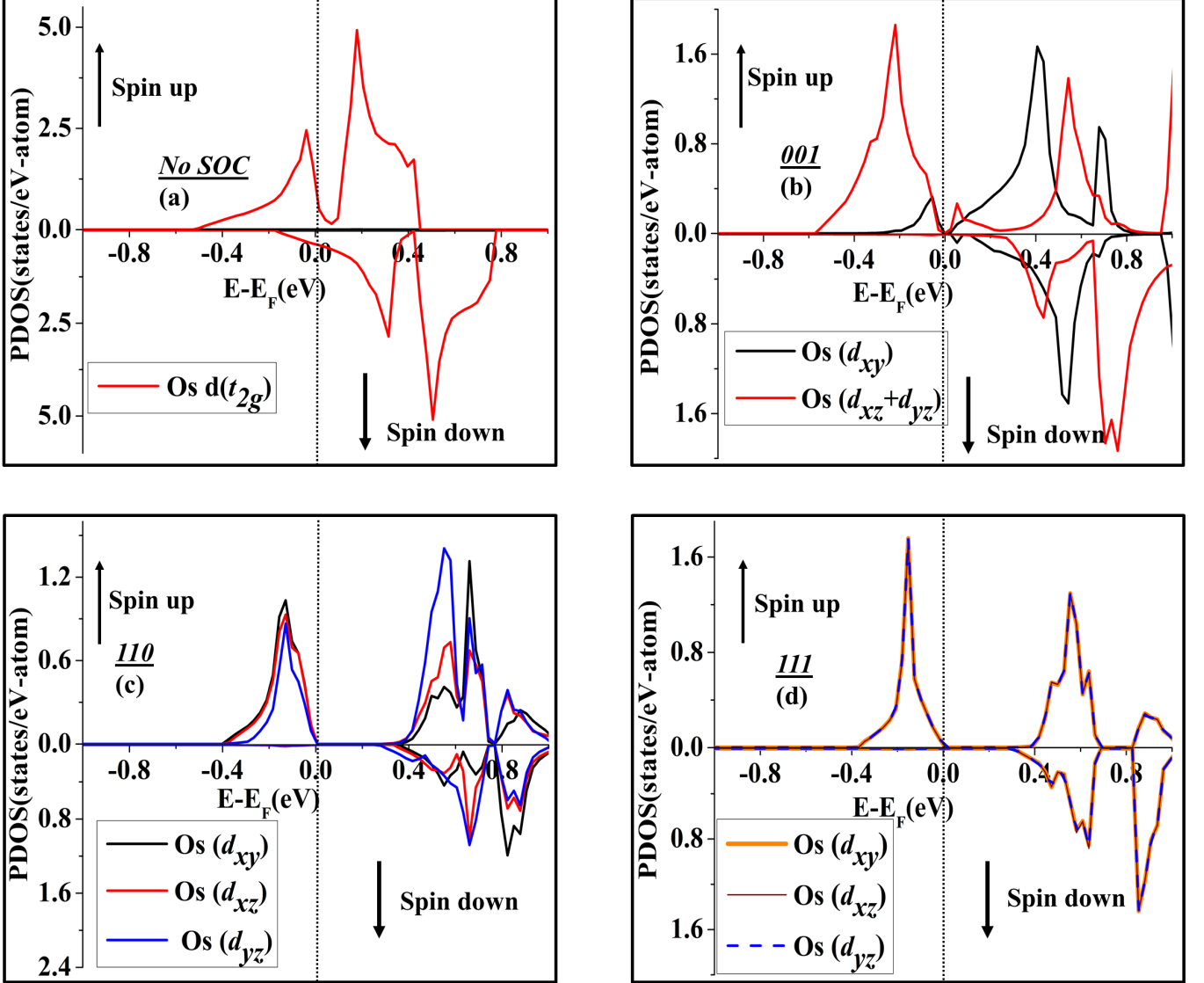


FIG. 1: Orbital-projected density of states plot for BNOO using the oeeHyb functional (a) without SOC, and for three different spin orbit coupling directions: (b) [001], (c) [110], and (d) [111]. The horizontal axis is in eV relative to the Fermi level (a), or top of the gap (b,c,d). The vertical axis is in states/eV-atom/formula unit. The most relevant information is the relative occupations of t_{2g} orbitals in the lower Hubbard band (-0.4 to 0.0 eV).

ting the lower (majority) and upper (minority) Hubbard bands is sufficiently large that the system remains essentially fully spin-polarized. The moment on Os is decreased by $0.07 \mu_B$ (see Table 1) by the rebonding induced by SOC. The orbital moment is around $-0.4 \mu_B$ for all directions of the moment, with the difference from unity being primarily due to half of the Wannier function lying on the O ions.

The PDOSs displayed in Fig. 1 indicate the character of the occupied orbital, and this figure clearly illustrates the large effect of SOC on the t_{2g} spectrum. For [001] spin direction, the dominance of d_{xz}, d_{yz} orbitals in the PDOS, along with the orbital moment reported in Table I, indicates occupation of the $d_{xz} - id_{yz} = d_{m=-1}$ orbital, with moment reduced due to the strong hybridization (hence partial quenching) with O $2p$ orbitals. For

[110], again d_{xz}, d_{yz} are equally occupied, however d_{xy} contributes somewhat more. For [111], all t_{2g} orbitals contribute equally, reflecting no evident symmetry breaking beyond that of choosing a specific [111] axis for the direction of magnetization. The occupied bandwidth in each case is 0.4 eV, though the differing shape of the band for the different directions of spin (discussed below) reflects the lowering of symmetry of the bands by SOC.

The relevant bands near the gap along selected symmetry directions are shown in Fig. 3 for each of the three directions of spin. These plots are shown for the 2% reduced lattice constant $a=8.10 \text{ \AA}$, for later comparison with BLOO. At the experimental volume, the results are extremely similar except that, for the [001] direction, the bands along W-K do not cross, leaving a small gap. The

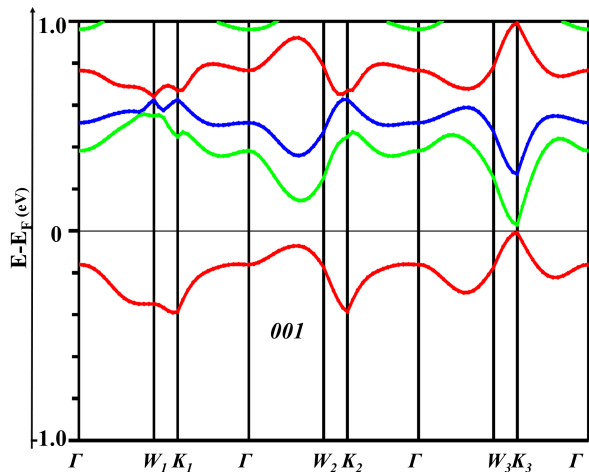


FIG. 2: Band plot along three different W-K directions for $\text{Ba}_2\text{NaOsO}_6$ with [001] magnetization axis ($a = 8.28 \text{ \AA}$), illustrating the large effect of symmetry lowering by the large spin-orbit interaction strength. The chosen points, in units of $\frac{\pi}{a}$, are $\Gamma = (0, 0, 0)$, $W_1 = (\frac{1}{4}, \frac{1}{4}, \frac{1}{2})$, $W_2 = (-\frac{1}{2}, \frac{1}{4}, -\frac{1}{4})$, $W_3 = (\frac{1}{2}, \frac{1}{4}, -\frac{1}{4})$, $K_1 = (\frac{3}{8}, 0, \frac{3}{8})$, $K_2 = (\frac{3}{8}, \frac{3}{8}, 0)$, $K_3 = (\frac{3}{8}, 0, -\frac{3}{8})$.

bands are quite flat through much of the zone (for example, along W-L- Γ directions), with important dispersion around the X point, and also dispersion along the W-K directions that is spin-direction dependent.

B. Magnetocrystalline anisotropy

The energy difference between [110] and [111] spin directions is small, and the band gaps for these two directions are indistinguishable. Fig. 1(b,c) illustrates the t_{2g} symmetry breaking due to SOC: for [001] d_{xz} and d_{yz} maintain equal occupation and dominate, each contributing 40% and obviously providing the orbital moment. There is also 20% d_{xy} , but without $d_{x^2-y^2}$ it cannot contribute to the orbital moment. For the easy axis [110] spin direction d_{xy} is also distinct from the other two, but interpreting the orbital moment in this global basis requires rotations with knowledge of phases. For the [111] spin direction all three orbitals contribute equally in the lower Hubbard band by symmetry.

From the calculated energies we obtain [110] as the easy axis, as determined experimentally.¹³ The [111] direction is very close in energy however ($\sim 1 \text{ meV}$, close to our precision), while the [001] direction is 13 meV higher. This agreement with experiment of the easy axis, following our success in reproducing the FM Mott insulating ground state, is an important validation of using the hybrid functional to model BNOO. The atom- and orbital-projected densities of states plot of Fig. 1 does not indicate directly the strong participation of O $2p$ orbitals in the nominal Os $5d$ bands, but this aspect has been emphasized in the earlier studies.^{18,21}

Including SOC lowers symmetry substantially so there are, for example, several different “X-W-K” directions

along the edge of the zone. Fig. 3 illustrates that there is actually a substantial change of dispersion along the zone boundary X-W-K directions, which disperse very differently for [001] compared to [111] and [110] spin directions. Otherwise the splitting of bands remains very similar, roughly 0.4 eV throughout the zone. In Fig. 2 the band plot for BNOO is shown along three inequivalent Γ -W-K directions for [001] magnetization direction. Along the W_3 - K_3 direction the band gap valence nearly vanishes (15 meV gap). With a decrease in lattice parameter, eventually the gap collapses, yielding an insulator-to-metal transition at a critical pressure, which is spin-direction dependent.

C. Pressure dependence

To access the effect of pressure we reduced the experimental lattice parameter of BNOO by 0.08 \AA , 0.18 \AA , and 0.42 \AA (1%, 2%, and 5% respectively) and repeated hybrid DFT calculations for the three magnetization directions. Table I provides the changes of the calculated band gap. For [001] orientation, band overlap and thus a insulator-metal transition (IMT) occurs. However, for [111] and [110] orientation the gap remains, having decreased by 30%. The relative energy difference is increased by the emergence of the metallic state, becoming several times higher than for the insulating states. From the bands plotted in a few symmetry directions in Fig. 3, collapse of the gap *per se* is not the reason for the IMT, rather it is the dispersion related to the direction of magnetization.

The dependence of the band dispersion on magnetization direction that is shown in Fig. 3 reveals a new kind of insulator-metal transition, one in which the tuning parameter is the magnetization direction. This direction can be manipulated by a sufficiently large applied field. Taken at face value, our modeling predicts that this type of transition will occur in BNOO, with an onset with pressure (decreasing volume) slightly below the experimental volume. The necessary pressure can be estimated using our calculated bulk modulus of $B = 50 \text{ GPa}$. Interpolating between our gap values at 8.28 \AA and 8.10 \AA (0.02 eV and -0.10 eV, respectively) give gap closing at $|\Delta a|/a \sim 4 \times 10^{-3}$, thus a gap closing and insulator metal transition in the vicinity of 5 kbar. Our characterization above of “at face value” refers to the well known issue that band gap values are uncertain at the level of several tenths of eV even when correlation corrections are made, and that the relation of oeeHyb band gaps to experimental values in correlated oxides is not established.

D. Similarities and differences: BNOO vs. BLOO

BLOO, the isostructural ($a = 8.10 \text{ \AA}$, $x_{\text{O}} = 0.2330$)¹⁴ and isovalent sister compound of BNOO, has an AFM ground state versus FM in BNOO. The primary difference seems

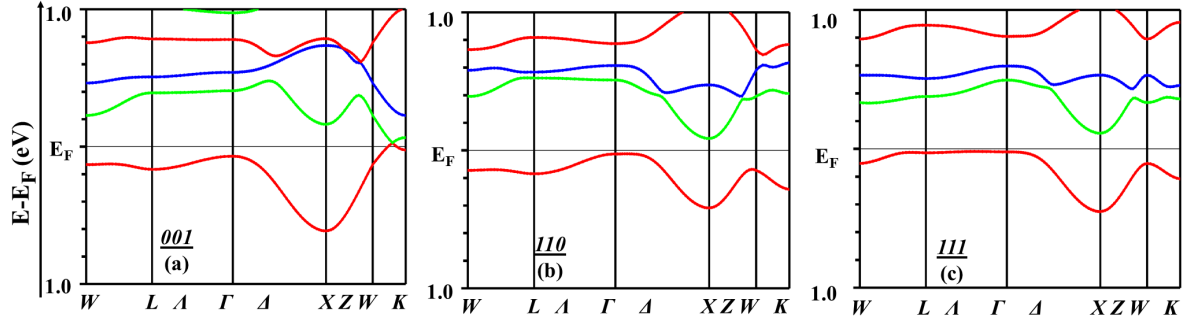
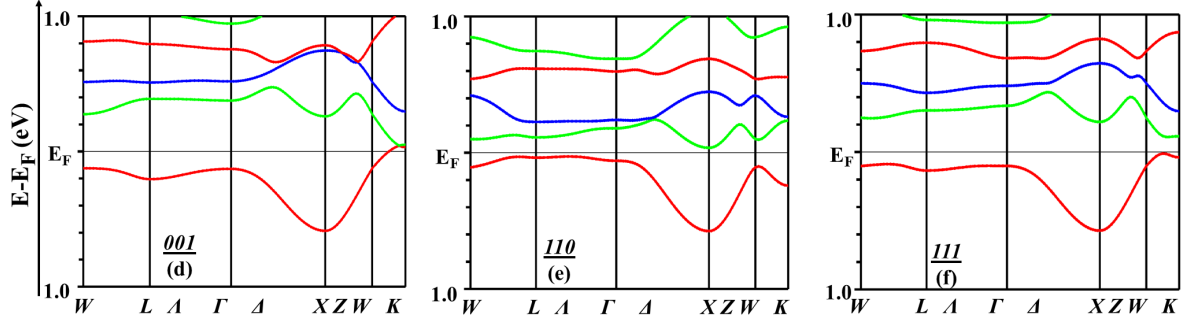
Ba₂NaOsO₆ ($A = 8.10$ Å) (a-c)**Ba₂LiOsO₆ ($A = 8.10$ Å) (d-f)**

FIG. 3: Band plots for Ba₂NaOsO₆ (a-c) and Ba₂LiOsO₆ (d-f) for the three directions of magnetization axis (indicated on the plots) and with a lattice parameter of 8.10 Å (experimental lattice parameter of Ba₂LiOsO₆). The differences are quite small for [001] but are important along W-X-K for the other two spin directions.

to be the Os-O distance, 1.81 Å versus 1.87 Å in BNOO. In the model of Chen¹ *et al.* that includes both intersite spin exchange J' and intersite Coulomb repulsion V , this structural difference suggests a larger V for BLOO. Given the similarities of the two band structures (thus, hopping amplitudes) and expected similarity of correlation strengths, J' may be the same for both compounds.

With strong SOC, the mechanism of magnetic ordering involves the tensorial coupling of spin+orbital moments,³² which lies beyond the scope of this paper. For purposes of comparison, we have performed all calculations for BLOO keeping ferromagnetic orientation to enable close comparison with BNOO. In Fig. 3 it is shown that, at a given volume, the band structures are similar over most of the zone. Because the gap is small, there are differences on the fine scale that are significant. At the experimental volume of BLOO, there is small band overlap along the plotted W-K direction for [001] magnetization direction for BNOO versus band touching (zero gap) for BLOO. Generally there are only visible differences in the vicinity of the W-K direction, which holds for other volumes that were studied.

It was mentioned above that the calculated easy axis of BNOO is [110], with [111] being close. This similarity of [110] and [111] energies persist for smaller lattice constants. The higher energy of [001] becomes even larger when the electronic structure becomes metallic, *i.e.* beyond the insulator-metal transition. For BLOO the easy

axis (assuming FM alignment) changes with volume: at the experimental volume [111] is the easy axis but at the BNOO lattice parameter (*i.e.* expanded by 0.18 Å) [001] becomes preferred. We note that the charge on Os is the same for both BNOO and BLOO for all volumes studied.

It can be seen, by comparing Table II with Table I, that the spin, orbital, and total moments on Os are affected somewhat by the Li/Na difference, consistent with the different behaviors seen experimentally. The differences can be appreciable and are both volume and spin-direction dependent. For example, the moment compensation is greatest for [111] polarization for both compounds ($\mu_{tot} = 0.07-0.08\mu_B$), but the greatest compensation occurs at different volumes (each at its own volume). There are differences in the band structures of BNOO and BLOO on the 0.1 eV scale, with BLOO generally having a somewhat smaller band gap. From Fig. 3 it is evident that the band structures differ strongly along several of the W-K directions.

V. DEPENDENCE OF SPIN DENSITY ON MAGNETIZATION DIRECTION

The PDOS plot of BNOO shows how degeneracy of Os t_{2g} orbitals (Fig. 1(a)) is broken when SOC is included. As already mentioned, Fig. 1(b) for [001] orientation shows that d_{xz} and d_{yz} predominates the occupied band,

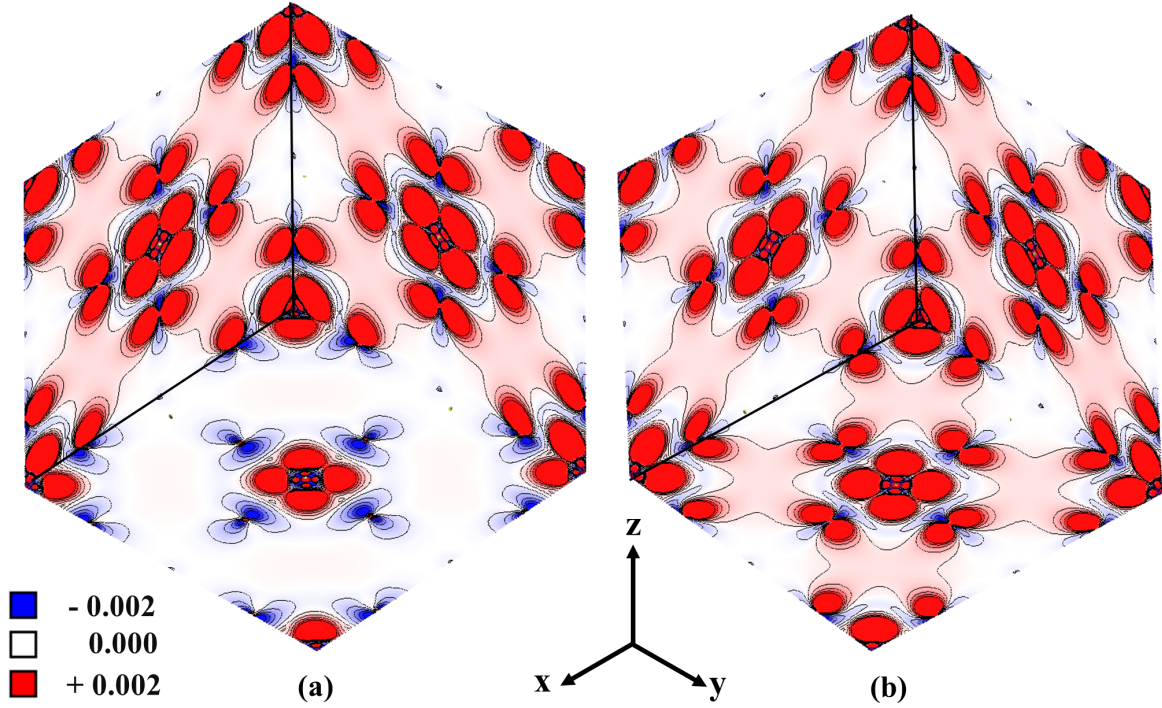


FIG. 4: Spin density contour plots in three planes, for $\text{Ba}_2\text{NaOsO}_6$ using the hybrid functional. Panel (a) corresponds to the [001] spin direction, panel (b) to the [111] spin direction. Os ions lie at the centers of the faces and at the corners, neighbored by four O ions in these planes. The blue contours in panel (a) reflect the negative spin polarization on the $2p_\sigma$ orbitals in the equatorial plane. See also Fig. 5. The figure was produced with the Xcrysden software.³³

with their complex combination ($m = -1$) accounting for the orbital moment. For illustration, Fig. 4(a,b) provides plots of the spin density contours in the three basal planes for [001] and [111] magnetization directions, to illustrate the differences. The spin density contours for [001] spin direction in the $y-z$ and $x-z$ planes are clearly very different from those in the $x-y$ plane, indicating its *strong anisotropy*. For the [111] orientation shown in Fig. 4(b), the spin density contours are equivalent in the three planes, reflecting the expected threefold symmetry. Some other symmetries will be absent, however.

Fig. 5 (left panel) provides a 3D isosurface plot as well as spin density contours (right panel) for the lower Hubbard band (occupied region at -0.4 eV to 0.0 eV) of BNOO at its ambient pressure volume, for [001] magnetization direction. The left panel reveals the $d_{xz} - id_{yz}$ spin density driven by SOC, which appears as large donuts around the Os site. The figure also shows the $p_x - ip_y$ spin density on the apical oxygen ions, which is driven by $p-d$ hybridization rather than direct SOC on oxygen (which is very weak for $Z=8$). This plot reinforces the earlier inferences about strong cubic symmetry breaking and additionally it shows that the contribution of d_{xz} , d_{yz} orbitals dominates the d_{xy} contribution.

The corresponding contour plot in Fig. 5 (right panel) provides more detail about the Os d_{xz} , d_{yz} orbitals hybridizing with p_z orbital of apical O, which thereby ac-

quires an orbital moment. The in-plane O p_z orbital (a p_π orbital) has substantial participation in bonding, but the p_z orbital contributes no orbital moment.

Finally, in Fig. 6 the spin density (which contributes the anisotropic charge density) is provided for both [110] and [111] orientations. For [111], the orbital is the $m_\ell = -1$ member of the symmetrized combinations of t_{2g} orbitals given by

$$\psi_m = \frac{1}{\sqrt{3}}(\zeta_m^0 d_{xy} + \zeta_m^1 d_{yz} + \zeta_m^2 d_{zx}), \quad (1)$$

where $\zeta_m = e^{2\pi mi/3}$ is the associated phase factor for threefold rotations. The spin density is anisotropic but not as strongly so as for [001] orientation.

Less intuitive and more surprising is the spin density for [110], also displayed in Fig. 6. By sight, it is very nearly cubic; the complex linear combination of t_{2g} orbitals necessary to provide the orbital moment is not at all evident in the spin density, which is a cube with rounded corners and dimpled faces. The spin density on the O ions is unremarkable and also nearly symmetric. This near-cubic symmetry provides an explanation for the lack of an observable Jahn-Teller distortion in this d^1 system.

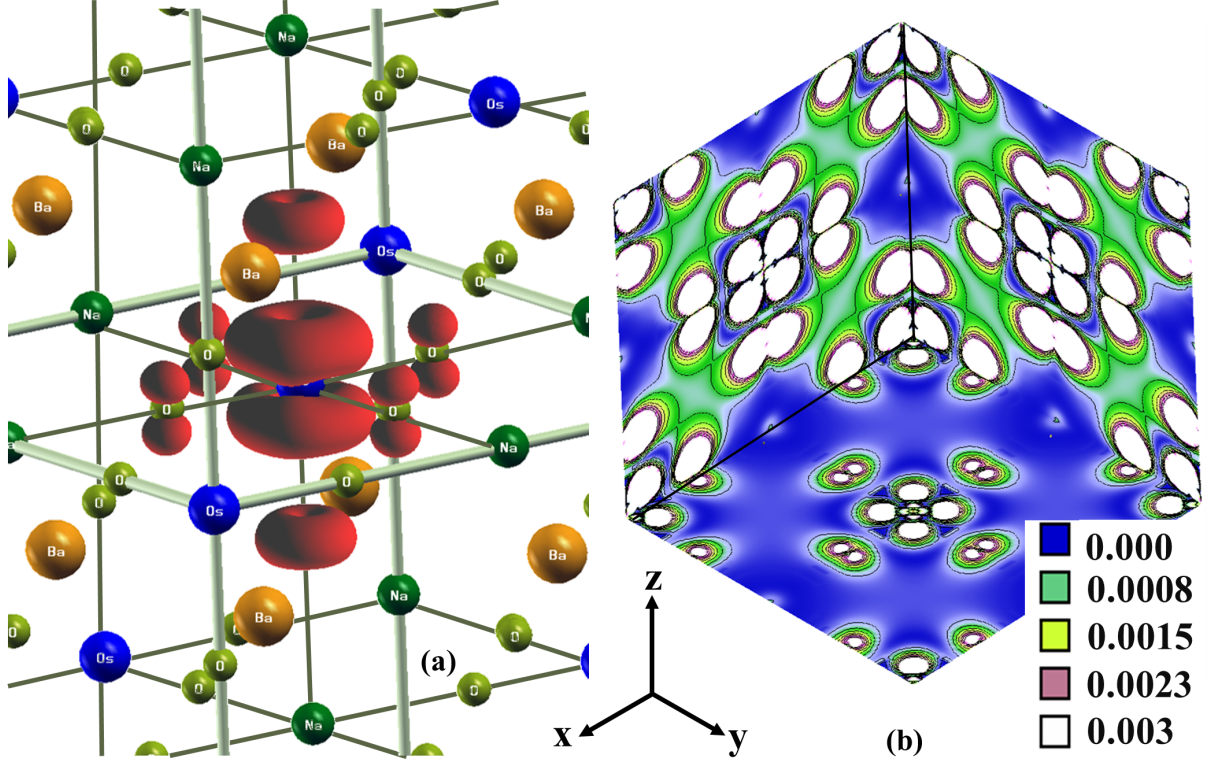


FIG. 5: Left panel: isocontour plot of the spin density in the limited range -04 eV to 0.0 eV – the occupied lower Hubbard band – for $\text{Ba}_2\text{NaOsO}_6$ at its experimental volume and [001] spin direction and using the hybrid DFT functional. This spin density is non-negative, in line with lack of any occupied minority spin, see Fig. 1. Right panel: isocontour plot of the same density, showing more detail. For example, the small spin density in the $x-y$ plane does not show up on the isocontour plot. The negative spin density on the equatorial O ions that is evident in Fig. 4 therefore arises due to the polarization of the O $2p$ bands (with no net moment).

A. Comments on magnetic moments

The orbital moment of Os is around $-0.4\mu_B$, with spin moment on Os about $0.5\mu_B$, for all volumes and spin directions we have studied. Thus the net moment is very small, only $0.1\mu_B$, on Os, and *most of the net (and observed) moment of $0.6\mu_B$ resides on the neighboring O ions*. For the [001] spin direction, the apical O acquires a spin moment three times larger than those in the equatorial plane, while for [110] the equatorial O ions have 1.5 larger spin. The spin density isocontours for spin along [001], shown in Fig 5, reveals its strong non-cubic symmetry.

Another unexpected feature arises from the calculation. For spin along [001], the apical O ion acquires an orbital moment approaching $0.1\mu_B$, whereas the in-plane O ions show negligible orbital moment. We are not aware of a significant orbital moment being detected, or predicted, on any oxygen ion. XMCD is the conventional measurement for obtaining the orbital moment, though tying it to the O ion will be challenging because there is substantial Os $5d$ character mixed with O $2p$, and vice versa. Detection of an orbital moment on O will help to substantiate the modeling of this unusual large SOC, $J_{\text{eff}} = \frac{3}{2}$ FM Mott insulator by the hybrid exchange func-

Method	μ_s	μ_l	μ_{tot}	Band Gap
Lattice parameter 8.28 Å				
oeeHyb	0.62	N/A	N/A	none
oeeHyb+SOC (001)	0.53	-0.40	0.13	0.02
oeeHyb+SOC (110)	0.56	-0.26	0.31	0.13
oeeHyb +SOC (111)	0.53	-0.32	0.22	0.09
Lattice parameter 8.10 Å				
oeeHyb	0.60	N/A	N/A	none
oeeHyb+SOC (001)	0.53	-0.39	0.13	none
oeeHyb +SOC (110)	0.52	-0.41	0.11	0.05
oeeHyb +SOC (111)	0.52	-0.44	0.08	0.06

TABLE II: Analogous to Table I, but for $\text{Ba}_2\text{LiOsO}_6$ and for only two lattice constants. Note: the total moment per f.u. will include an $\sim 0.55\mu_B$ spin moment not included within the Os sphere, thus primarily on the oxygen ions.

tional, as well as generalize expectations of where orbital magnetism may emerge.

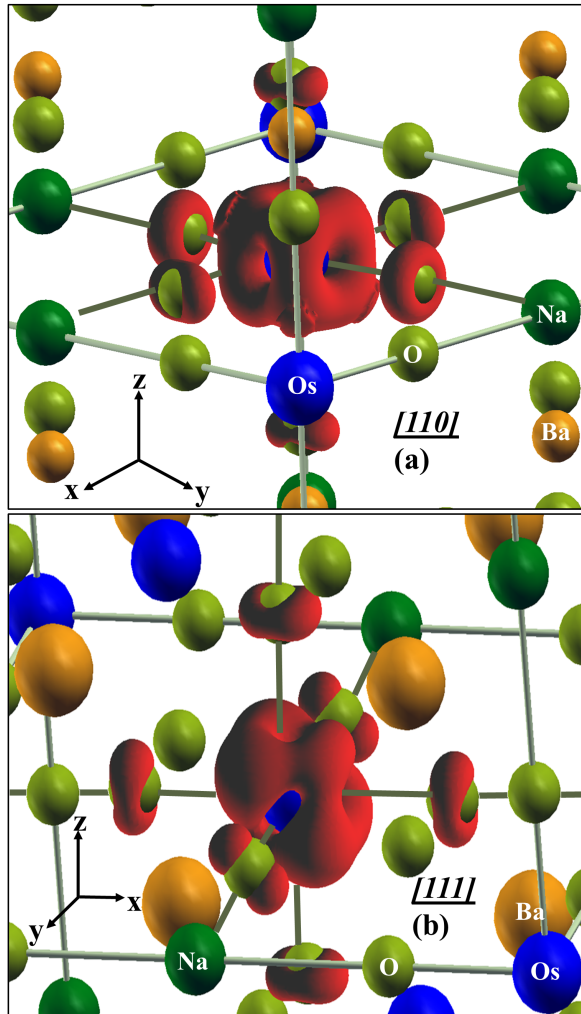


FIG. 6: Isosurface plot of the spin density of BNOO as in Fig. 5, but for [110] (top panel) and [111] (bottom panel) spin orientation. Note the near-cubic symmetry of the [110] density on both the Os ion and the neighboring O ions. The [111] density shows three-fold symmetry around the chosen [111] axis for an $m_\ell = \pm 1$ orbital for Eq. 1.

VI. SUMMARY

The hybrid density functional has been used for the modeling of $\text{Ba}_2\text{NaOsO}_6$ with considerable success. Un-

like our attempts with GGA+U+SOC, when SOC is included, and only then, it provides a robust FM Mott insulating ground state for the moment aligned along any of the three symmetry directions. Thus BNOO (and BLOO) is a $J_{\text{eff}} = \frac{3}{2}$ Mott insulator at quarter filling, driven by the combination of strong exchange-correlation and large SOC. Though the spin magnetization remains completely spin-up when SOC is included, the large changes in the composition of the occupied orbital are driven by SOC. On the scale of 0.1-0.2 eV which is important considering the small gap, the band structure is strongly dependent of the orientation of the magnetization.

In addition, our approach predicts the [110] direction as the easy axis, as observed, though [111] is close in energy. The character of the net moment is unexpected. On the one hand, the spin and orbital moments on Os are 0.5 and $-0.4\mu_B$, respectively, leaving a net moment on Os of $0.1\mu_B$, similar to earlier indications.^{18,21} However this value leaves most of the total moment of $0.6\mu_B$ arising from the oxygen ions in the OsO_6 cluster. The observed ordered moment is $\sim 0.2\mu_B$ thus indicates somewhat larger compensation, or small spin contribution, than our results provide.

Another unusual feature found here is that for spin along [001], there is a $0.1\mu_B$ orbital moment on the apical oxygen ion. This surprisingly large value cannot arise from the very small SOC on oxygen; rather it is the hybridization of the Os $d_{xz} - id_{yz}$ combination with the $p_x - ip_y$ orbital that transfers orbital angular momentum to O. This effect does not operate for other spin orientations.

VII. ACKNOWLEDGMENTS

We acknowledge many useful conversations with K.-W. Lee, discussions with I. R. Fisher, R. T. Scalettar, and N. J. Curro, and comments on the manuscript from R. T. Scalettar. Our research used resources of the National Energy Research Scientific Computing Center (NERSC), a DOE Office of Science User Facility supported by the Office of Science of the U.S. Department of Energy under Contract No. DE-AC02-05CH11231. This research was supported by DOE Stockpile Stewardship Academic Alliance Program under Grant DE-FG03-03NA00071.

¹ G. Chen, R. Pereira, and L. Balents, Phys. Rev. B. **82**, 174440 (2010).

² G. Jackeli and G. Khaliullin, Phys. Rev. Lett. **102**, 017205 (2009).

³ B. J. Kim, H. Jin, S. J. Moon, J.-Y. Kim, B.-G. Park, C. S. Leem, J. Yu, T.W. Noh, C. Kim, S.-J. Oh, J. H. Park, V. Durairaj, G. Cao, and E. Rotenberg, Phys. Rev. Lett. **101**, 076402 (2008).

⁴ S. J. Moon, H. Jin, K.W. Kim, W. S. Choi, Y. S. Lee, J. Yu, G. Cao, A. Sumi, H. Funakubo, C. Bernhard, and

T.W. Noh, Phys. Rev. Lett. **101**, 226402 (2008).

⁵ B. J. Kim, H. Ohsumi, T. Komesu, S. Sakai, T. Morita, H. Takagi, and T. Arima, Science **323**, 1329 (2009).

⁶ G. Cao, T. F. Qi, L. Li, J. Terzic, S. J. Yuan, L. E. DeLong, G. Murthy, and R. K. Kaul, Phys. Rev. Lett. **112**, 056402 (2014).

⁷ A. A. Aczel, D. E. Bugaris, J. Yeon, C. de la Cruz, H.-C. zur Loye, and S. E. Nagler, Phys. Rev. B. **88**, 014413 (2013).

⁸ A. A. Aczel, P.J. Baker, D. E. Bugaris, J. Yeon, H.-C. zur

- Loye, T. Guidi, and D. T. Adroja, *Phys. Rev. Lett.* **112**, 117603 (2014).
- ⁹ A. A. Aczel, D. E. Bugaris, L. Li, J.-Q. Yan, C. de la Cruz, H.-C. zur Loye, and S. E. Nagler, *Phys. Rev. B* **87**, 014435 (2013).
 - ¹⁰ K. Yamamura, M. Wakeshima, and Y. J. Hinatsu, *Solid State Chem.* **179**, 605 (2006).
 - ¹¹ Y.-J. Song, K.-H. Ahn, K.-W. Lee, and W. E. Pickett, arXiv:14087.4078.
 - ¹² A. J. Steele, P. J. Baker, T. Lancaster, F. L. Pratt, I. Franke, S. Ghannadzadeh, P. A. Goddard, W. Hayes, D. Prabhakaran, and S. J. Blundell, *Phys. Rev. B* **84**, 144416 (2011).
 - ¹³ A. S. Erickson, S. Misra, G. J. Miller, R. R. Gupta, Z. Schlesinger, W. A. Harrison, J. M. Kim, and I. R. Fisher, *Phys. Rev. Lett.* **99**, 016404 (2007).
 - ¹⁴ K. E. Stitzer, M. D. Smith, and H.-C. Z. Loye, *Solid State Science* **4**, 311 (2002).
 - ¹⁵ W. R. Gemmill, M. D. Smith, R. Prozorov, and H.-C. zur Loye, *Inorg. Chem.* **44**, 2639 (2005).
 - ¹⁶ Y. Shi, Y. Guo, Y. Shirako, W. Yi, X. Wang, A. A. Belik, Y. Matsushita, H. L. Feng, Y. Tsujimoto, M. Arai, N. Wang, M. Akaogi, and K. Yamaura, *J. Am. Chem. Soc.* **135**, 44 (2013).
 - ¹⁷ M.-C. Jung, Y.-J. Song, K.-W. Lee, and W. Pickett, *Phys. Rev. B* **87**, 115119 (2013).
 - ¹⁸ K. W. Lee and W. E. Pickett, *EPL* **80**, 37008 (2007).
 - ¹⁹ T. Shirakawa, H. Watanabe, and S. Yunoki, *J. Phys.: Conf. Series* **400**, 032088 (2012).
 - ²⁰ J. Zhang, K. Haule, and D. Vanderbilt, *Phys. Rev. Lett.* **111**, 246402 (2013).
 - ²¹ H. J. Xiang and M.-H. Whangbo, *Phys. Rev. B* **75**, 052407 (2007).
 - ²² P. Blaha, K. Schwarz, G. Madsen, D. Kvasicka, and J. Luitz, WIEN2k, An Augmented Plane Wave + Local Orbitals Program for Calculating Crystal Properties, Technical University of Vienna, Vienna, (2001). We have used version 12 of Wien2k, because we have found that SOC with the hybrid functional does not always work correctly in version 13.
 - ²³ F. Tran, P. Blaha, K. Schwarz, and P. Novák, *Phys. Rev. B* **74**, 155108 (2006).
 - ²⁴ P. Novák, J. Kuneš, L. Chaput, and W. E. Pickett, *Phys. Stat. Sol. B* **243**, 563 (2006).
 - ²⁵ In the Wien2k case.inorb file the flag HYBR is used for Os 5d orbitals, with a fraction of 0.25.
 - ²⁶ J. P. Perdew, K. Burke, and M. Ernzerhof, *Phys. Rev. Lett.* **77**, 3865 (1996).
 - ²⁷ J. Heyd, G. E. Scuseria, and M. Ernzerhof, *J. Chem. Phys.* **118**, 8207 (2003).
 - ²⁸ G. Kresse and J. Furthmüller, *Phys. Rev. B* **54**, 11169 (1996).
 - ²⁹ H.-J. Kim, J.-H. Lee, and J.-H. Cho, *Sci. Rep.* **4**, 5253 (2014) DOI:10.1038/srep05253.
 - ³⁰ A. H. MacDonald, W. E. Pickett, and D. D. Koelling, *J. Phys. C* **13**, 2675 (1980).
 - ³¹ K.-W. Lee (private communication).
 - ³² S.-T. Pi, R. Nanguneri, and S. Y. Savrasov, *Phys. Rev. Lett* **112**, 077203 (2014).
 - ³³ A. Kokalj, *J. Mol. Graphics Modell.* **17**, 176 (1999), A. Kokalj, *Comp. Mater. Sci.*, **28**, 155 (2003).